Programmable Nanolithography with Plasmon Nanoparticle Arrays

A. Femius Koenderink,*,† Jesus V. Hernández,‡ Francis Robicheaux,‡ L. D. Noordam,§ and Albert Polman†

FOM Institute AMOLF, Center for Nanophotonics, Kruislaan 407, NL-1098SJ Amsterdam, The Netherlands, Department of Physics, Auburn University, Auburn, Alabama 36849, and Van der Waals−Zeeman Institute, Valckenierstraat 65, NL-1018XE, Amsterdam, The Netherlands

ABSTRACT

We describe how optical contact lithography based on plasmon particle array masks allows generation of a large number of different subwavelength exposure patterns using a single mask. Within an exact point dipole model, we study the local response of silver particles in small two-dimensional arrays with 50−200 nm spacing. We show how illumination with unfocused light allows optically addressing particles either individually or in controlled configurations; which pattern will be exposed by the mask is programmed by varying the wavelength, incidence angle, and polarization of the incident wave.

Photolithography is one of the most widely used techniques in micro- and nanofabrication and is an enabling technology both in industrial semiconductor processing and in the recent progress of nanoscience. Because photolithography relies on far-field imaging, the smallest achievable feature size is limited by the diffraction limit. Creating nanometer features with photolithography is therefore generally associated with a reduction in wavelength, either by using extreme UV photons or by using solid immersion in high refractive index media to reduce the wavelength. To remove the diffraction limit as a bottleneck for nanofabrication altogether, many alternative approaches are being pursued, including non-optical techniques like nanoimprinting[1] and near-field optical techniques. These approaches include surface plasmon interference nanolithography[2−4] and imaging through silver superlenses.[5,6] For all of these near-field approaches, the diffraction limit is removed, but a second paradigm of photolithography remains: that a single mask is used only for a single pattern.

Silver and gold nanoparticles that have a plasmon resonance at visible wavelengths are well-known for their ability to strongly enhance electric field intensities in their immediate vicinity,[7] which can be used for near-field pattern transfer[8] and nanolithography.[9] In a recently reported experiment,[10] Hubert et al. first illuminated nanoparticles embedded in photoresist and imaged this enhanced near-field a posteriori

by mapping the deformation of the resist using atomic force microscopy. Essentially, this experiment demonstrates that the near-field of a single nanoparticle is sufficiently localized to allow silver nanoparticles to be useful in near-field optical lithography masks.[9,10] In this work, we present calculations that show that one can in fact controllably create many distinct patterns of hot spots from a single lithography mask, which can be both a one- and a two-dimensional (2D) plasmon particle array. The pattern is programmed via the parameters of the illuminating plane wave. The physics behind these phenomena is that closely spaced particles in an array couple[11,12] via both near- and far-field dipolar interactions. As in an antenna optimized for receiving a radio signal, the coherent coupling of all the fields can be tuned to controllably create a hot spot of constructive interference on a single or a few dipoles depending on array geometry and illumination conditions, as was first proposed for linear arrays by Hernández et al.[13] Recently, we experimentally demonstrated the effectiveness of such coupling to create wavelength-tunable hot spots in linear plasmon particle arrays.[14] The realization that coherent coupling between mask features occurs in lithography schemes for ultrasmall feature sizes will have a significant impact on any type of optical nanolithography: On the one hand, mask design is highly nontrivial because no intuitive correspondence between mask and exposure exists. On the other hand, letting go of the paradigm that a single mask be used only for a unique pattern brings the freedom to create a single, reusable, generic mask to expose many desired patterns by varying the illumination.
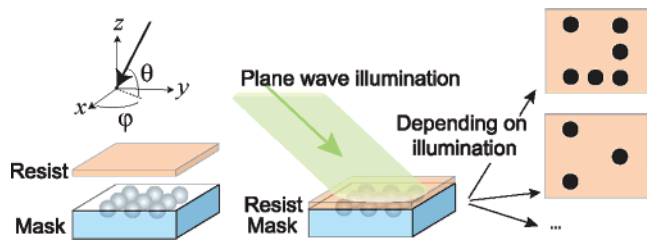
Figure 1 shows a schematic of the process that we study: we consider a transparent mask containing an array of silver

* Corresponding author. E-mail: f.koenderink@amolf.nl. Telephone: +31 20 6081234. Fax: +31 20 6684106.
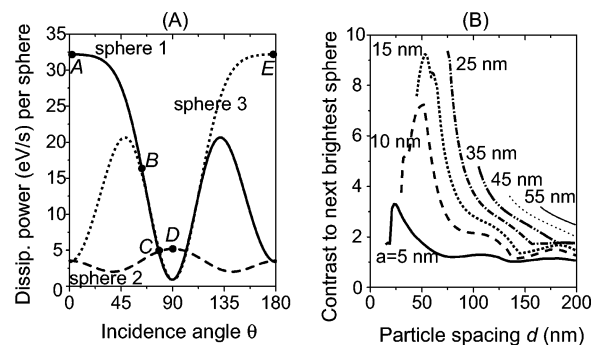† FOM Institute AMOLF.
‡ University of Auburn.
§ Van der Waals−Zeeman Institute.

Figure 1. We consider a transparent mask (refractive index 1.5) containing a configuration of closely spaced silver nanoparticles. Resist is pressed onto this mask and illuminated using unfocused light. A high field intensity, and hence an exposure in the resist, is created on certain combinations of particles. Which combinations are addressed can be controlled by the wavelength, polarization, and incidence angle of the incident light. The upper left inset shows the coordinate system used throughout this work. The mask is in the xy plane. The incident direction is specified by the angle θ relative to the mask normal and the angle φ in the plane of the resist.

Figure 2. (A) We consider the dissipated power per sphere (at 1V/cm incident field) for nanospheres in a linear array of 3 silver particles ($a = 25$ nm radius, $d = 75$ nm spacing in glass ($n = 1.5$)) illuminated with a 500 nm wavelength plane wave incident and polarized in the $\varphi = 0$ plane. The spheres are located on the x-axis (coordinate system defined in Figure 1). As the incident angle θ is scanned, the distribution of power over the spheres changes (solid line: sphere 1 at $x = -d$ farthest from the incident direction at $\theta = 0$; dashed line: middle sphere (sphere 2 at $x = 0$); dotted line: sphere 3 at $x = d$ closest to the incident beam at $\theta = 0$) and allows different exposure patterns. For $\theta = 0°$ and 180°, power localizes on a single end sphere. (B) Contrast of the end sphere relative to the next brightest nanoparticle as a function of particle spacing for different particle radii a as labeled. For each particle spacing, the wavelength was optimized and θ was kept at 0 for optimum contrast of the end particle. For spacings in the range from 25 to 150 nm, a useful contrast for programmable plasmon lithography is obtained.

particles close to the mask surface. After this mask is brought into contact with photoresist, the resist is exposed to an incident plane wave. A high field intensity is created only near the silver particles, resulting in a pattern of strongly localized exposed dots. The length scale of this pattern is the particle spacing, which can be much smaller than the incident wavelength. By varying the illumination wavelength, polarization, and incidence angle, this single mask can give rise to different exposures. To model the optical response of nanoparticle array masks, we use a well-known point-dipole model[13,15−17] that is valid for particle spacings d larger than 3 times the particle radius a.[18] The particles are described as point dipoles with a resonant polarizability that is based on a Drude model for the dielectric constant of silver, which was fitted to optical constants in Palik.[17,19] As in refs (17,20), the polarizability includes radiation damping to maintain a proper energy balance[21] and a dynamic depolarization term to account for the retardation-induced red-shift of the resonance with increasing particle radius.[22] It is essential that the model contains both the near-field and the retarded far-field of the dipoles and takes into account the coupling between all particles in addition to the driving of all particles by the incident light.[13,15−17] Without these terms, the model would reduce to the quasistatic model,[12] which does not reproduce antenna effects such as the desired excitation of single dots in larger arrays.[13,17] Given an incident plane wave, we obtain the induced dipole moments **p** on all of the particles and calculate the electric field intensity at the photoresist−mask interface.

To illustrate the concept of programmable lithography, we first consider a linear array of three silver particles of radius 25 nm, spaced by 75 nm and embedded in a transparent mask (refractive index $n = 1.5$, assumed equal to that of the substrate). Figure 2A shows the response $|\mathbf{p}|^2$ (more precisely, the Ohmic dissipated power,[13] which is directly proportional to $|\mathbf{p}|^2$) of all three spheres to plane wave illumination at a fixed wavelength of $\lambda = 500$ nm as a function of the angle of incidence. The solid curve corresponds to the response of the sphere farthest away from the incident beam at incident angle $\theta = 0$, while the dashed curve represents the response of the central sphere, and the dotted curve that of the sphere

closest to the incident beam at $\theta = 0$. When the angle of incidence is along the array axis (points labeled A and E in Figure 2), the excitation on the sphere farthest from the incident direction exceeds that on the other spheres by a factor ~10. As the incident beam is rotated toward the normal, the sphere closest to the incident direction also acquires a significant excitation; around $\theta = 45°$, the spheres at both ends are equally excited, while the middle sphere remains a factor of five darker (labeled B in Figure 2). Close to normal incidence, all three curves cross, indicating that all three spheres are equally excited (C). Exactly at normal incidence (D), the middle sphere carries an excitation more than 5 times stronger than the spheres at the two endpoints. Figure 2A shows that, in a lithography scheme in which a contrast of 1−5 suffices to differentiate between exposed and unexposed, all distinct patterns (all binary combinations where any sphere is either dark or bright), except for the patterns with one endpoint dark, can be made using unfocused light of a single wavelength simply by rotating the incoming beam. The remaining pattern can be generated by changing the illumination wavelength and polarization (not shown).

From Figure 2A, we conclude that in subwavelength nanoparticle arrays, distinct configurations of particles can be controllably addressed even though all particles are irradiated. The key to this phenomenon is to use the parameters of the incident beam to control the relative phases with which particles are excited in order to control the destructive interference that keeps some particles dark and the constructive interference that gives rise to hot spots on other particles. Because the basis for this programmable addressability is interference, the addressability is expected

to be sensitive to the particle *spacing* in the mask, which sets the minimum feature size for lithography. In Figure 2B, we consider the range of geometrical parameters in which particles can be individually addressed. As a figure of merit, we consider the ratio of the power $|\mathbf{p}|^2$ on the brightest end-point particle at $\theta = 0°$ relative to that on the next brightest particle as a measure of contrast. Figure 2B shows this contrast as a function of particle spacing for different particle sizes, where we have optimized the wavelength to obtain maximum contrast for each spacing and particle size. Excellent contrasts above 3 are obtained for particles with radii between 5 and 30 nm and particle spacings between 25 and 150 nm. Generally, we find that larger particle sizes result in a red-shift of the wavelength of optimum operation, consistent with the well-known red-shift of the first (dipolar) Mie resonance with increasing particle size. For a given particle size, the optimum wavelength is not strongly dependent on particle arrangement. Both for 1D arrays and for 2D arrays, the wavelength range for programmable lithography coincides with the single particle plasmon resonance line width. One can therefore control the wavelength range for programmable lithography by tuning the single particle resonance, either through the mask refractive index, the particle size, or the choice of metal.[20] For silver particles, the wavelength of operation can be shifted from 400 to 600 nm by tuning the mask index from 1.3 to 1.6.

Having demonstrated that programmable addressability of plasmon particles in subwavelength arrays can be achieved at high contrast for a large range of feature sizes, we will now consider the utility of this individual addressability for lithography applications. To this end, we consider 2D particle arrangements. To quantitatively establish the usefulness for lithography, one has to define contrast criteria, which will depend on the response of photoresist to the local electric field intensity $|\mathbf{E}|^2$ near the plasmon particles. Furthermore, one needs a scheme to define and classify the set of target patterns that can be produced with a given mask. Both the contrast criteria and the pattern classification scheme are most easily defined by focusing on a single parameter per particle to quantify the local exposure, which is the induced dipole moment $|\mathbf{p}|.^2$ Given an illumination geometry, we classify the distribution of $|\mathbf{p}|^2$ according to the following criteria: (i) A site counts as "exposed" if its dipole moment $|\mathbf{p}|^2$ is at least a fraction β of that on the brightest particle. (ii) A site is "unexposed" if its dipole moment $|\mathbf{p}|^2$ is smaller than a fraction δ of the dipole moment on the brightest particle (i.e., when $|\mathbf{p}|^2$ is at most a fraction δ/β of the weakest exposed particle). (iii) If any particle in the array cannot be classified as exposed or unexposed, the illumination conditions are not considered to give rise to a valid pattern for lithography.

In Figure 3, we consider all symmetry-distinct patterns that can be exposed by illuminating a 2×2 square mask of silver particles (radius 25 nm, spacing 75 nm) with linearly polarized light under various angles. Taking symmetry into account, the 2^4 binary combinations of four particles that can be exposed or unexposed reduce to five inequivalent patterns with at least one particle exposed. Assuming contrast parameters $\beta = 90\%$ and $\delta = 25\%$, illumination conditions
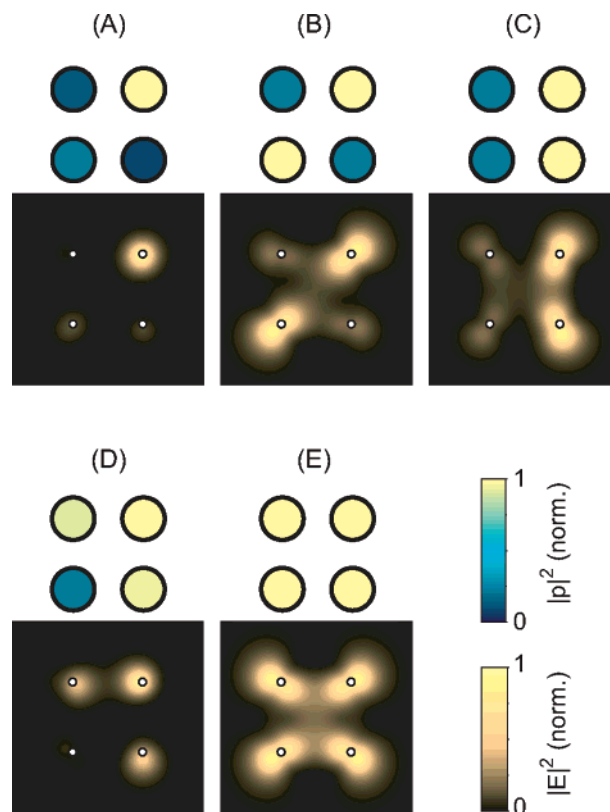
Figure 3. For a mask containing a 2×2 array of Ag particles (spacing 75 nm), all conceivable combinations of particles can be addressed individually. The filled-in dots show the relative amount of excitation on each sphere (gray scale); the contour plots show the resulting electric field intensity in a plane just 5 nm above the mask; the location of the spheres is indicated by open circles. Incidence conditions are listed in the text.

exist for all five patterns that allow exposure in a single step. For instance, Figure 3 shows that a single sphere can be exposed by illuminating with a plane wave of any wavelength between 530 and 600 nm that is incident within the plane of the square along the square diagonal, with a polarization that is normal the mask plane. The sphere farthest from the incident direction will be exposed. If the incident wave vector is not chosen in the plane of the particle array, but normal to the plane of particles, the symmetric patterns in Figure 3B and E can be created using any wavelength between 530 and 585 nm and setting the polarization to be along the diagonal to be exposed B, or along any edge of the square E. The tolerance in orientation of the polarization and in the wave vector is only ~3° for the pattern in E with all spheres exposed, compared to about ~20° for the case with one diagonal exposed in B. Exposing two adjacent spheres, as in C, requires off-normal illumination (θ between 0° (in the plane of the spheres) and about 60°) with electric field vector oriented along the row of spheres that is to be illuminated; as for the pattern in A, the exposed spheres are away from the direction of incidence. The most difficult pattern to create in terms of tolerances on the illumination parameters is the one with three spheres exposed and one unexposed (Figure 3D). Within the visibility criteria that we have chosen, this pattern can only be created in a narrow wavelength window from 595 to 600 nm for wave vectors *close to* the array
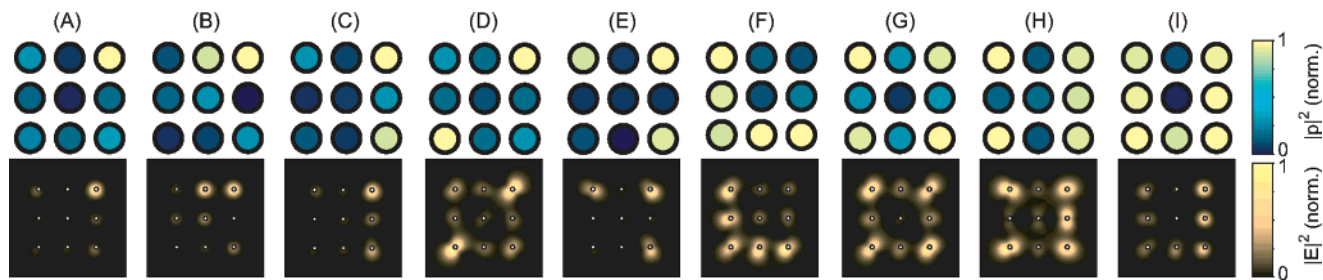
Figure 4. For a mask containing a 3 × 3 array of Ag particles (spacing 75 nm), 9 out of 138 conceivable combinations of particles can be addressed individually. Other configurations can only be exposed sequentially. The filled dots show the relative amount of excitation on each sphere (gray scale); the contour plots show the resulting electric field intensity in a plane just 5 nm above the mask.

diagonal *nearly in* the plane of the mask, and for *approximately* in-plane polarization. For all these factors (polarization, azimuthal, and polar incidence angle), the illumination geometry needs to be between roughly 2° and 5° away from the symmetric configuration: otherwise the pattern with a single exposed dot is generated, or an invalid pattern results with two exposed dots on the diagonal and two dots with $\delta < |\mathbf{p}|^2 < \beta$.

The asymmetric incidence condition required to create a pattern of three dots in a single exposure is clearly reflected in the plots in Figure 3 of the electric field intensity $|\mathbf{E}|^2$ in a plane just above the nanospheres, which represents the mask−photoresist interface. In all cases, we find qualitatively that the electric field intensity $|\mathbf{E}|^2$ is strongly localized at the spheres that are classified as exposed and that the field intensity is small at the unexposed spheres. This conclusion supports our choice to analyze $|\mathbf{p}|^2$ to quantify the potential of particle arrays for programmable lithography. A more detailed inspection of the field patterns shows several subtleties relevant for lithography. From the field patterns, one clearly discerns that configuration A in Figure 3 corresponds to a single strongly excited dipole that is oriented out of the plane, while the patterns B, C, and E correspond to dipoles that are all oriented within the plane of the mask. Dipole orientations out of the plane of the mask give rise to a more strongly localized field at the interface between mask and resist, and hence a potentially higher resolution. For dipoles within the plane of the mask, the exposed spots are also localized at the mask particles, but they are anisotropic. For configurations A−C and E, illumination conditions along symmetry directions of the square can be used, resulting in symmetric field patterns. For the pattern in Figure 3D in which exactly three spheres carry a large dipole moment, the field pattern has several remarkable properties due to the asymmetric illumination geometry. First, it appears that the three areas of large field near the spheres are not clearly anisotropic, even though the induced dipoles do have an in-plane component. Second, these areas of large field are slightly shifted by about 7 nm relative to the sphere positions. A third surprise is that a small difference for the dipole strengths of the exposed particles (normalized $|\mathbf{p}|^2$ of 0.91, 1, and 0.94 in clockwise order starting from the upper left sphere) translates into a large difference in field strength (maximum normalized $|\mathbf{E}|^2$ near particle 0.53, 1.0, and 0.6, respectively). The field intensity distribution is the result of interfering contributions of the individual dipoles: the

asymmetric excitation conditions required to create a balanced distribution of $|\mathbf{p}|^2$ cause an asymmetric distribution in the phases and the orientations of the dipoles. For the configuration in Figure 3D, the in-plane dipole components are approximately in phase, while the larger out-of-plane components are nearly out of phase. The larger asymmetry in $|\mathbf{E}|^2$ is due to a partial cancellation of these out-of-plane components, which effectively magnifies the small differences in dipole moments. Instead of optimizing the contrast in $|\mathbf{p}|^2$, one can also optimize the contrast in $|\mathbf{E}|^2$, or in the average of $|\mathbf{E}|^2$ over an area comparable to the sphere size. For the pattern in D, we find a range of illumination angles close to those that optimize the contrast in $|\mathbf{p}|^2$, which give rise to a more useful field pattern (normalized $|\mathbf{E}|^2$ near the exposed (unexposed) particles within 90% (25%) of $|\mathbf{E}|^2$ at the brightest particle) even though the dipole moments do not meet the contrast criterium (normalized $|\mathbf{p}|^2$ of 0.93, 1, and 0.55 for the "exposed particles" and 0.27 for the "unexposed" particle). The overall conclusion is that the excitation of arbitrary dipole combinations is indeed possible in 2 × 2 square arrays of dipoles. The correspondence between the distribution of dipole moments and the field intensity at the mask−photoresist interface is not trivial due to polarization and interference effects. While in many cases the distribution of dipole moments is a good predictor for the exposure, in some cases, an explicit optimization for $|\mathbf{E}|^2$ at the photoresist surface is required.

Finally, we consider a 2D mask consisting of a square of 3 × 3 particles. Such a mask is surprisingly more complex than a 2 × 2 mask: while there are five distinct patterns for a 2 × 2 array, there are 138 (symmetry-distinct) patterns in the case of a 3 × 3 array. Keeping the same contrast criterion $\beta = 90\%$ and $\delta = 25\%$ as before, 7 out of the 138 patterns can be generated, which are the patterns A,D−I in Figure 4. When the contrast criterion is relaxed to $\delta = 33\%$, 9 out of 138 patterns (also B and C) can be exposed. On the one hand, Figure 4 shows that a considerable variety of useful patterns can be created in a single illumination step. On the other hand, not every conceivable pattern can be generated with single-step *plane wave* illumination. A valid question is whether one can build any pattern with sequential illuminations. With sequential illumination, one should control the cumulative dose for each mask site, putting more stringent demands on δ if a particle is to remain unexposed throughout all illumination steps. For a 3 × 3 mask, the available patterns do not suffice to create all possible

configurations by sequential exposure because two single-particle configurations are inaccessible according to Figure 4: the central particle and the center particles on each side of the square cannot be addressed with plane wave illumination. Instead, one needs to employ multiple phase-related beams simultaneously or to apply phase-shaping and coherent control techniques to a single illumination beam.[23]

Regarding practical implementations of this scheme, we note that the feasibility of lithography has essentially been demonstrated for *single* particles in refs 9 and 10. We therefore focus on challenges for practical applications that are specific for masks of *multiple* particles. A first challenge will be to overcome the effects of mask imperfections on the reproducible programming of exposures. A 5% variation in particle size causes a 15% variation in its polarizability, i.e., in the dipole moment $|\mathbf{p}|$ induced by incident light. Therefore, fluctuations in the mask can cause large deviations from the programmed pattern. However, the programmability of the mask itself allows compensating for fluctuations in the mask by adapting the illumination parameters to the mask. If a mask is reused many times, a single calibration step before using it is not problematic. A second major challenge is the scaling of the programming problem with mask size. Even if it is possible to address every conceivable pattern in a given mask in a single illumination step, the complexity of classifying all patterns and finding the appropriate illumination required for each pattern scales at a daunting rate with the size of the mask: taking symmetry into account, the number of distinct patterns that exist for an $N \times N$ square array of particles is approximately 2^{N^2-2}, whereas the parameter space for a single incident plane wave is only five-dimensional (wavelength λ, incoming angles θ and φ, as well as a single complex coefficient for mixing the two polarization channels). However, the combinatorial complexity of large masks need not be an obstacle for programmable lithography. First, a mask need not be an $N \times N$ square array of particles but could be designed to contain only a few desired structures that one can choose from using the illumination conditions. This design freedom encompasses both the particle arrangement and the particle sizes, which need not be the same for all particles in the mask. Second, the exponential growth of the programming problem with mask size could be circumvented by sequentially illuminating subunits of the mask using weakly focused light. Because the resolution is decoupled from the wavelength, the demands on focus size need not be stringent. Third, we note that reciprocity in Maxwell's equations allows one to reduce the complexity of finding illumination conditions that give a certain pattern and obviates the need for brute force searching of a parameter space in which most parameters will not give rise to the desired pattern. According to reciprocity, a strongly frequency- and direction-selective receiving antenna is an equally selective radiating element. Thus, a configuration in which a few dipoles respond strongly to a certain external illumination will radiate strongly into the same direction when the dipoles are driven as emitters in proportion to their desired response to the external field. This principle is analogous to "time-reversed acoustics",

where a localized sound excitation can be reconstructed by first recording the emission of a point source at several locations and then switching the role of emitter and recorders.[24] In the point-dipole model, one can simply set up a desired configuration of exposed and unexposed particles, and calculate the far-field radiation pattern. In this case, one optimizes the relative phases of the bright dipoles to obtain the most directed radiation pattern, which by reciprocity corresponds most closely to a single beam exposure. While the dimension of the parameter space is potentially much larger than the number of beam parameters, it can be a significant advantage that all parameters in the parameter space give rise to the desired pattern.

References

(1) Chou, S. Y.; Krauss, P. R.; Renstrom, P. J. *Science* **1996**, *272*, 85−87.
(2) Luo, X.; Ishihara, T. *Appl. Phys. Lett.* **2004**, *84*, 4780−4782.
(3) Liu, Z. W.; Wei, Q. H.; Zhang, X. *Nano Lett.* **2005**, *5*, 957−961.
(4) Shao, D. B.; Chen, S. C. *Appl. Phys. Lett.* **2005**, *86*, 253107.
(5) Fang, N.; Lee, H.; Zhang, X. *Science* **2005**, *308*, 534−537.
(6) Pendry, J. B. *Phys. Rev. Lett.* **2000**, *85*, 3966−3969.
(7) Genov, D. A.; Sarychev, A. K.; Shalaev, V. M.; Wei, A. *Nano Lett.* **2004**, *4*, 153−158.
(8) Ono, A.; Kato, J.-I.; Kawata, S. *Phys. Rev. Lett.* **2005**, *95*, 267407.
(9) Kik, P. G.; Maier, S. A.; Atwater, A. *Mat. Res. Soc. Symp. Proc.* **2002**, *705*, Y3.6.
(10) Hubert, C.; Rumyantseva, A.; Lerondel, G.; Grand, J.; Kostcheev, S.; Billot, L.; Vial, A.; Bachelot, R.; Royer, P.; Chang, S. H.; Gray, S. K.; Wiederrecht, G. P.; Schatz, G. C. *Nano Lett.* **2005**, *5*, 615−619.
(11) Quinten, M.; Leitner, A.; Krenn, J. R.; Aussenegg, F. R. *Opt. Lett.* **1998**, *23*, 1331−1333.
(12) Brongersma, M. L.; Hartman, J. W.; Atwater, H. A. *Phys. Rev. B* **2000**, *62*, R16356−R16359.
(13) Hernández, J. V.; Noordam, L. D.; Robicheaux, F. *J. Phys. Chem B* **2006**, *109*, 15808−15811.
(14) Waele, R.; Koenderink, A. F.; Polman, A. **2006**, unpublished results.
(15) Weber, W. H.; Ford, G. W. *Phys Rev B* **2004**, *70*, 125429.
(16) Citrin, D. S. *Nano Lett.* **2005**, *5*, 985−989.
(17) Koenderink, A. F.; Polman, A. *Phys. Rev. B*, **2006**, *74*, 033402.
(18) Park, S. Y.; Stroud, D. *Phys. Rev. B*, **2004**, *69*, 125418.
(19) Palik, E. D. Ed., *Handbook of Optical Constants of Solids*; Academic: Orlando, FL, 1985.
(20) Kelly, K. L.; Coronado, E.; Zhao, L. L.; Schatz, G. C. *J. Phys. Chem. B* **2003**, *107*, 668−677.
(21) de Vries, P.; van Coevorden, D. V.; Lagendijk, A. *Rev. Mod. Phys.* **1998**, *70*, 447−466.
(22) Meier, M.; Wokaun, A. *Opt. Lett.* **1983**, *8*, 581−583.
(23) Stockman, M. I.; Faleev, S. V.; Bergman, D. J. *Phys. Rev. Lett.* **2002**, *88*, 067402.
(24) Fink, M.; Cassereau, D.; Derode, A.; Prada, C.; Roux, P.; Tanter, M.; Thomas, J.-L.; Wu, F. *Rep. Prog. Phys* **2000**, *63*, 1933−1955.